

Realization of a three-dimensional photonic topological insulator

Yihao Yang^{1,2,3,4}, Zhen Gao^{3,4,}, Haoran Xue^{3,4}, Li Zhang^{1,2}, Mengjia He^{1,2}, Zhaoju Yang^{3,4}, Ranjan Singh^{3,4}, Yidong Chong^{3,4}, Baile Zhang^{3,4,*} and Hongsheng Chen^{1,2,*}*

¹State Key Laboratory of Modern Optical Instrumentation and The Electromagnetics Academy at Zhejiang University, Zhejiang University, Hangzhou 310027, China.

²Key Laboratory of Micro-Nano Electronics and Smart System of Zhejiang Province, College of Information Science and Electronic Engineering, Zhejiang University, Hangzhou 310027, China.

³Division of Physics and Applied Physics, School of Physical and Mathematical Sciences, Nanyang Technological University, 21 Nanyang Link, Singapore 637371, Singapore.

⁴Centre for Disruptive Photonic Technologies, The Photonics Institute, Nanyang Technological University, 50 Nanyang Avenue, Singapore 639798, Singapore.

*Correspondence to: gaozhen@ntu.edu.sg, blzhang@ntu.edu.sg, hansomchen@zju.edu.cn

ABSTRACT

Three-dimensional (3D) topological insulators are phases of quantum matter that have a bulk bandgap, while also exhibiting gapless surface states that behave as two-dimensional (2D) massless Dirac fermions. Recently, a new type of 3D photonic crystal, a classical analogue of a 3D topological insulator, was predicted theoretically. Here, we experimentally demonstrate a 3D photonic crystal with a complete topological bandgap of extremely wide ($> 25\%$) bandwidth. The sample consists of split-ring resonators with strong magneto-electric coupling, and behaves as a “weak topological insulator”, or a stack of 2D quantum spin Hall insulators. Using direct field measurements, we map out both the gapped bulk bandstructure and the Dirac-like dispersion of the photonic surface states. Our work extends the family of 3D topological insulators from fermions to bosons, and paves the way for applications in topological photonic cavities, circuits, and lasers in 3D geometries.

Photonic bandgap materials, also known as photonic crystals, are materials possessing a bandgap that forbids the propagation of electromagnetic waves (i.e., light waves governed by the classical Maxwell equations) in all directions. While electronic bandgaps are a long-established concept, it was only in the late 1980s that photonic bandgap materials were theoretically predicted (1, 2), and then experimentally realized in the form of a three-dimensional (3D) photonic crystal with a complete bandgap at microwave frequencies (3). Subsequent researchers have realized 3D photonic crystals at optical frequencies (4, 5), and shown that optical cavities and circuits can be formed by embedding point, line, or volume defects in a 3D photonic crystal (6, 7).

During the past two decades, condensed matter physics has been revolutionized by the introduction of topological classifications of phases of matter (8, 9). A 3D topological insulator has a bulk bandgap, similar to a conventional insulator, but conducts on its surface due to the existence of topological surface states, which behave as two-dimensional (2D) massless Dirac fermions that are robust against backscattering (8, 9). Thus far, classical wave analogues of topological insulators have been limited to 2D (10-13). In 3D, topologically nontrivial Weyl bandstructures have been demonstrated in classical systems; these are *ungapped*, but support topological surface states that are unprotected from scattering into the bulk (14-17). Recently, there have been several theoretical proposals for realizing a 3D topological bandgap in photonics (18-22). One uses high-index magneto-optic materials to generate a bandstructure analogous to a “strong” topological insulator (which has topological surface states on all surfaces), albeit one with an incomplete bandgap; this has, however, proven challenging to fabricate (19). Another recent proposal involves a photonic “weak” topological insulator (WTI), which has topological surface states on some but not all surfaces (20). WTIs emerge from stacking layers of 2D quantum spin Hall insulators with appropriate interlayer couplings (23). Although WTI surface states were originally considered to be unprotected against disorder, recent research has revealed that they are robust against disorder, so long as time-reversal symmetry and the existence of the bandgap are maintained (24, 25).

Here, we report on the realization of a 3D photonic topological insulator (PTI) with a WTI bandstructure, featuring a complete and extremely wide topological bandgap. We have experimentally mapped out the bulk bandstructure, as well as the dispersion of the surface states along an internal domain wall. We show explicitly that the surface states have the predicted form

of a Dirac cone (20). Unlike the proposal of Slobozhanyuk et al. (20), the present design utilizes a 3D array of metallic split-ring resonators (SRRs). The structure is fabricated from metal and dielectric materials (which are non-magneto-optical, so the system is time-reversal symmetric apart from negligible dissipative losses). The resonance-enhanced bianisotropy (magneto-electric coupling) of the SRRs plays a role analogous to the strong spin-orbit coupling in topological insulator materials (8, 9), allowing for a topological bandgap with width $> 25\%$. This exceeds even previously-demonstrated topological bandgap widths in 2D, which have been 10% or less (11, 26-34), and substantially exceeds the gap widths in previous 3D proposals, which were on the order of a few percent and/or incomplete (18-22).

We start with a photonic crystal design featuring an ungapped bandstructure with 3D Dirac points. As depicted in Fig. 1a, the photonic crystal has a unit cell consisting of six connected metallic SRRs (35). The crystal is formed by arranging the unit cells in a triangular lattice in the x-y plane, as shown in Fig. 1b, and stacking identical layers along the z direction. The background material is Teflon woven glass fabric copper-clad laminate, with relative permittivity 2.5. Note that the back-to-back arrangement of the SRRs cancels the bianisotropy at the K and K' points in the Brillouin zone (36). The lattice has a mirror ($z \rightarrow -z$) symmetry, which we denote by σ_z . For fine-tuned lattice parameters, the photonic bandstructure exhibits frequency-isolated 3D Dirac points (20, 37) (i.e., doubly-degenerate Weyl points), with four-fold degeneracy at the band-crossing points at K and K', as shown in Fig. 1d.

Our design for a wide-gap PTI is shown in Fig. 1c. These SRRs are *not* arranged back-to-back, and σ_z is broken. This unit cell can be formed by removing the upper three SRRs in the unit cell of Fig. 1a and adjusting the z periodicity accordingly. The resultant bandstructure is shown in Fig. 1e, and exhibits a wide ($> 25\%$) bandgap. Although the relationship between the two photonic crystal designs is not immediately obvious, we show in the Supplemental Material, Section 1 that the bandgap in Fig. 1e is continuously deformable into the infinitesimal bandgap opened at the Dirac points when the σ_z symmetry of Fig. 1a is perturbatively broken. In the original σ_z -symmetric structure, the electric and magnetic dipoles have opposite parity and form decoupled modes under in-plane propagation ($k_z = 0$). Breaking σ_z induces a bianisotropic coupling between the in-plane electric and magnetic dipoles, generating two hybrid modes in each of the lower and upper bands. Near the K and K' valleys, the pair of eigenmodes within each band have electric and

magnetic components that are respectively in-phase or out-of-phase, corresponding to pseudo-spin-up or pseudo-spin-down, for both lower and upper bands (20, 30, 38, 39). This form of bianisotropic coupling has previously been shown to play a role analogous to the Kane-Mele spin-orbit coupling in quantum spin Hall materials (8, 9, 20, 38, 39). Detailed modal analysis can be found in the Supplemental Materials, Section 2.

The PTI is shown in Fig. 2a. The sample was fabricated with printed circuit board technology by etching 5 mm-thick dielectric laminates with double-sided (0.035 mm thick) copper cladding. Each printed layer is paired with a 0.65 mm-thick dielectric spacer. At the centre of each unit cell is an air hole of radius 1.5 mm, allowing an electromagnetic probe to be inserted to measure the fields within the crystal. The sample consists of 40 identical layers, stacked along the z axis, and is fabricated with a domain wall separating two photonic crystal domains with opposite σ_z -breaking (i.e., the SRRs in the two domains are oriented upside-down relative to each other), as shown in Fig. 2a-b. The domain wall thus lies in the y - z plane (marked by a red dotted line in Fig. 2a), with size 45×40 unit cells.

In the first set of experiments, illustrated in Fig. 2b, a dipole source antenna is inserted from the bottom center of the y - z plane, indicated by the red (blue) dotted line, 4 unit cells into the bulk; a second dipole antenna, acting as the probe, is inserted inside the sample from the hole marked with a red (blue) dot in Fig. 2a, at the depth of 8 unit cells into the bulk, to measure the transmission of the surface (bulk) states. The whole sample is wrapped with microwave absorbers. The frequency dependence of the transmittance, along the domain wall and in the bulk, is shown in Fig. 2c. We observe an approximately 20 dB drop in the transmittance of the bulk states, extending from approximately 4.3 GHz to 6.0 GHz, corresponding to a bulk bandgap. Along the domain wall, however, the transmittance remains high throughout the frequency range, indicating the existence of surface states. Our numerical results also demonstrate pseudospin-momentum locking along the isofrequency contours of the surface Dirac cone, which is another important property of 3D PTIs (Supplemental Materials, Section 3).

To probe the bulk bandstructure, we measure the electromagnetic response in the y - z plane (indicated by the blue dotted line in Fig. 2a) away from the domain wall. The probe dipole antenna is fixed to a robotic arm, and we map the field intensities in the selected plane. After Fourier transformation to reciprocal space, we obtain the plot shown in Fig. 2d, which closely matches the

numerically-computed projected bandstructure shown in Fig. 2e. In particular, we observe a complete photonic bandgap in the bulk, with almost the same frequency range of the bandgap in Fig. 2c.

Next, we repeat the field measurements with the source and probe located along the 2D domain wall. The surface bandstructure, shown in Fig. 3a, reveals a family of surface states that span the frequency range of the bulk bandgap, forming a conical dispersion curve. The surface Dirac point occurs at 5.1 GHz, near the mid-point of the bulk bandgap, and along the Γ -X high-symmetry line (near the projection of the K point of the 3D Brillouin zone). A second Dirac point near K' is not shown in this plot. The isofrequency plots in the 2D reciprocal space confirm that the dispersion is indeed conical, as shown in the insets of Fig. 3a. These results closely match the numerically computed surface bandstructure, as shown in Fig. 3b. By placing the probes in adjacent unit cells, away from the domain wall, we verify that the surface states are tightly confined to the domain wall with penetration depth of around 10.3 mm; details are given in the Supplemental Materials, Section 4.

Our work thus demonstrates a classical electromagnetic analogue of a 3D topological insulator. This versatile table-top platform can be used to simulate relativistic Dirac fermions, as well as to undertake detailed experimental studies of PTI surface state robustness, which is the subject of considerable theoretical interest. The realization of such a wide 3D photonic bandgap opens the door to a wide range of novel topological photonic devices, such as topological photonic cavities, circuits, and lasers (27, 28) in 3D geometries. Although the current study has focused on realizing a photonic crystal for the manipulation of electromagnetic waves, a similar lattice design may be applied to other bosonic systems, such as acoustic and mechanical structures (13).

ACKNOWLEDGEMENTS

We thank Q. Yan at Zhejiang University, L. Lu at the Chinese Academy of Sciences, and J. C. W. Song at Nanyang Technological University for helpful discussions. The work at Zhejiang University was sponsored by the National Natural Science Foundation of China under Grant Nos. 61625502, 61574127, 61601408, 61775193 and 11704332, the ZJNSF under Grant No. LY17F010008, the Top-Notch Young Talents Program of China, the Fundamental Research Funds

for the Central Universities under Grant No. 2017XZZX008-06, and the Innovation Joint Research Center for Cyber-Physical-Society System. Y. D. Chong and B. Zhang acknowledge the support of Singapore Ministry of Education under Grants No. MOE2015-T2-1-070, MOE2015-T2-2-008, MOE2016-T3-1-006 and Tier 1 RG174/16 (S). Y. Yang and R. Singh acknowledge the support of Singapore Ministry of Education under Grants No. MOE2015-T2-2-103.

REFERENCES AND NOTES

1. E. Yablonovitch, Inhibited spontaneous emission in solid-state physics and electronics. *Phys. Rev. Lett.* **58**, 2059 (1987).
2. S. John, Strong localization of photons in certain disordered dielectric superlattices. *Phys. Rev. Lett.* **58**, 2486 (1987).
3. E. Yablonovitch, T. Gmitter, K. Leung, Photonic band structure: The face-centered-cubic case employing nonspherical atoms. *Phys. Rev. Lett.* **67**, 2295 (1991).
4. S.-y. Lin, J. Fleming, D. Hetherington, B. Smith, R. Biswas, K. Ho, M. Sigalas, W. Zubrzycki, S. Kurtz, J. Bur, A three-dimensional photonic crystal operating at infrared wavelengths. *Nature* **394**, 251 (1998).
5. A. Blanco, E. Chomski, S. Grabtchak, M. Ibsate, S. John, S. W. Leonard, C. Lopez, F. Meseguer, H. Miguez, J. P. Mondia, Large-scale synthesis of a silicon photonic crystal with a complete three-dimensional bandgap near 1.5 micrometres. *Nature* **405**, 437 (2000).
6. S. A. Rinne, F. García-Santamaría, P. V. Braun, Embedded cavities and waveguides in three-dimensional silicon photonic crystals. *Nature Photon.* **2**, 52 (2008).
7. M. Qi, E. Lidorikis, P. T. Rakich, S. G. Johnson, J. Joannopoulos, E. P. Ippen, H. I. Smith, A three-dimensional optical photonic crystal with designed point defects. *Nature* **429**, 538 (2004).
8. X.-L. Qi, S.-C. Zhang, Topological insulators and superconductors. *Reviews of Modern Physics* **83**, 1057 (2011).
9. M. Z. Hasan, C. L. Kane, Colloquium: topological insulators. *Reviews of Modern Physics* **82**, 3045 (2010).
10. L. Lu, J. D. Joannopoulos, M. Soljačić, Topological photonics. *Nature Photon.* **8**, 821 (2014).
11. A. B. Khanikaev, G. Shvets, Two-dimensional topological photonics. *Nature Photon.* **11**, 763 (2017).
12. T. Ozawa, H. M. Price, A. Amo, N. Goldman, M. Hafezi, L. Lu, M. Rechtsman, D. Schuster, J. Simon, O. Zilberberg, Topological Photonics. *arXiv preprint arXiv:1802.04173*, (2018).
13. R. Süsstrunk, S. D. Huber, Observation of phononic helical edge states in a mechanical topological insulator. *Science* **349**, 47-50 (2015).
14. B. Yang, Q. Guo, B. Tremain, R. Liu, L. E. Barr, Q. Yan, W. Gao, H. Liu, Y. Xiang, J. Chen, C. Fang, A. Hibbins, L. Lu, S. Zhang, Ideal Weyl points and helicoid surface states in artificial photonic crystal structures. *Science* **359**, 1013-1016 (2018).
15. L. Lu, Z. Wang, D. Ye, L. Ran, L. Fu, J. D. Joannopoulos, M. Soljačić, Experimental observation of Weyl points. *Science* **349**, 622-624 (2015).
16. H. Wang, L. Zhou, Y. Chong, Floquet Weyl phases in a three-dimensional network model. *Phys. Rev. B* **93**, 144114 (2016).
17. J. Noh, S. Huang, D. Leykam, Y. Chong, K. P. Chen, M. C. Rechtsman, Experimental observation of optical Weyl points and Fermi arc-like surface states. *Nature Physics* **13**, 611 (2017).
18. V. Yannopapas, Gapless surface states in a lattice of coupled cavities: A photonic analog of topological crystalline insulators. *Phys. Rev. B* **84**, 195126 (2011).
19. L. Lu, C. Fang, L. Fu, S. G. Johnson, J. D. Joannopoulos, M. Soljačić, Symmetry-protected topological photonic crystal in three dimensions. *Nature Physics* **12**, 337 (2016).
20. A. Slobzhanyuk, S. H. Mousavi, X. Ni, D. Smirnova, Y. S. Kivshar, A. B. Khanikaev, Three-dimensional all-dielectric photonic topological insulator. *Nature Photon.* **11**, 130 (2017).
21. Q. Lin, X.-Q. Sun, M. Xiao, S.-C. Zhang, S. Fan, Constructing three-dimensional photonic topological insulator using two-dimensional ring resonator lattice with a synthetic frequency dimension. *arXiv preprint arXiv:1802.02597*, (2018).
22. T. Ochiai, Gapless surface states originating from accidentally degenerate quadratic band touching in a three-dimensional tetragonal photonic crystal. *Phys. Rev. A* **96**, 043842 (2017).

23. L. Fu, C. L. Kane, E. J. Mele, Topological insulators in three dimensions. *Phys. Rev. Lett.* **98**, 106803 (2007).
24. R. S. Mong, J. H. Bardarson, J. E. Moore, Quantum transport and two-parameter scaling at the surface of a weak topological insulator. *Phys. Rev. Lett.* **108**, 076804 (2012).
25. Z. Ringel, Y. E. Kraus, A. Stern, Strong side of weak topological insulators. *Phys. Rev. B* **86**, 045102 (2012).
26. S. Barik, A. Karasahin, C. Flower, T. Cai, H. Miyake, W. DeGottardi, M. Hafezi, E. Waks, A topological quantum optics interface. *Science* **359**, 666-668 (2018).
27. M. A. Bandres, S. Wittek, G. Harari, M. Parto, J. Ren, M. Segev, D. N. Christodoulides, M. Khajavikhan, Topological insulator laser: Experiments. *Science* **359**, eaar4005 (2018).
28. B. Bahari, A. Ndao, F. Vallini, A. El Amili, Y. Fainman, B. Kante, Nonreciprocal lasing in topological cavities of arbitrary geometries. *Science* **358**, 636-640 (2017).
29. M. Hafezi, E. A. Demler, M. D. Lukin, J. M. Taylor, Robust optical delay lines with topological protection. *Nature Physics* **7**, 907 (2011).
30. X. Cheng, C. Jouvaud, X. Ni, S. H. Mousavi, A. Z. Genack, A. B. Khanikaev, Robust reconfigurable electromagnetic pathways within a photonic topological insulator. *Nature Mater.* **15**, 542 (2016).
31. S. Yves, R. Fleury, T. Berthelot, M. Fink, F. Lemoult, G. Lerosey, Crystalline metamaterials for topological properties at subwavelength scales. *Nat. Commun.* **8**, 16023 (2017).
32. F. Gao, Z. Gao, X. Shi, Z. Yang, X. Lin, H. Xu, J. D. Joannopoulos, M. Soljačić, H. Chen, L. Lu, Probing topological protection using a designer surface plasmon structure. *Nat. Commun.* **7**, 11619 (2016).
33. W.-J. Chen, S.-J. Jiang, X.-D. Chen, B. Zhu, L. Zhou, J.-W. Dong, C. T. Chan, Experimental realization of photonic topological insulator in a uniaxial metacrystal waveguide. *Nat. Commun.* **5**, 5782 (2014).
34. Z. Wang, Y. Chong, J. D. Joannopoulos, M. Soljačić, Observation of unidirectional backscattering-immune topological electromagnetic states. *Nature* **461**, 772 (2009).
35. J. B. Pendry, A. J. Holden, D. Robbins, W. Stewart, Magnetism from conductors and enhanced nonlinear phenomena. *IEEE Trans. Microw. Theory Tech.* **47**, 2075-2084 (1999).
36. R. Marqués, F. Medina, R. Rafii-El-Idrissi, Role of bianisotropy in negative permeability and left-handed metamaterials. *Phys. Rev. B* **65**, 144440 (2002).
37. Q. Guo, B. Yang, L. Xia, W. Gao, H. Liu, J. Chen, Y. Xiang, S. Zhang, Three dimensional photonic Dirac points in metamaterials. *Phys. Rev. Lett.* **119**, 213901 (2017).
38. T. Ma, A. B. Khanikaev, S. H. Mousavi, G. Shvets, Guiding electromagnetic waves around sharp corners: topologically protected photonic transport in metawaveguides. *Phys. Rev. Lett.* **114**, 127401 (2015).
39. A. B. Khanikaev, S. H. Mousavi, W.-K. Tse, M. Kargarian, A. H. MacDonald, G. Shvets, Photonic topological insulators. *Nature Mater.* **12**, 233 (2013).

FIGURES

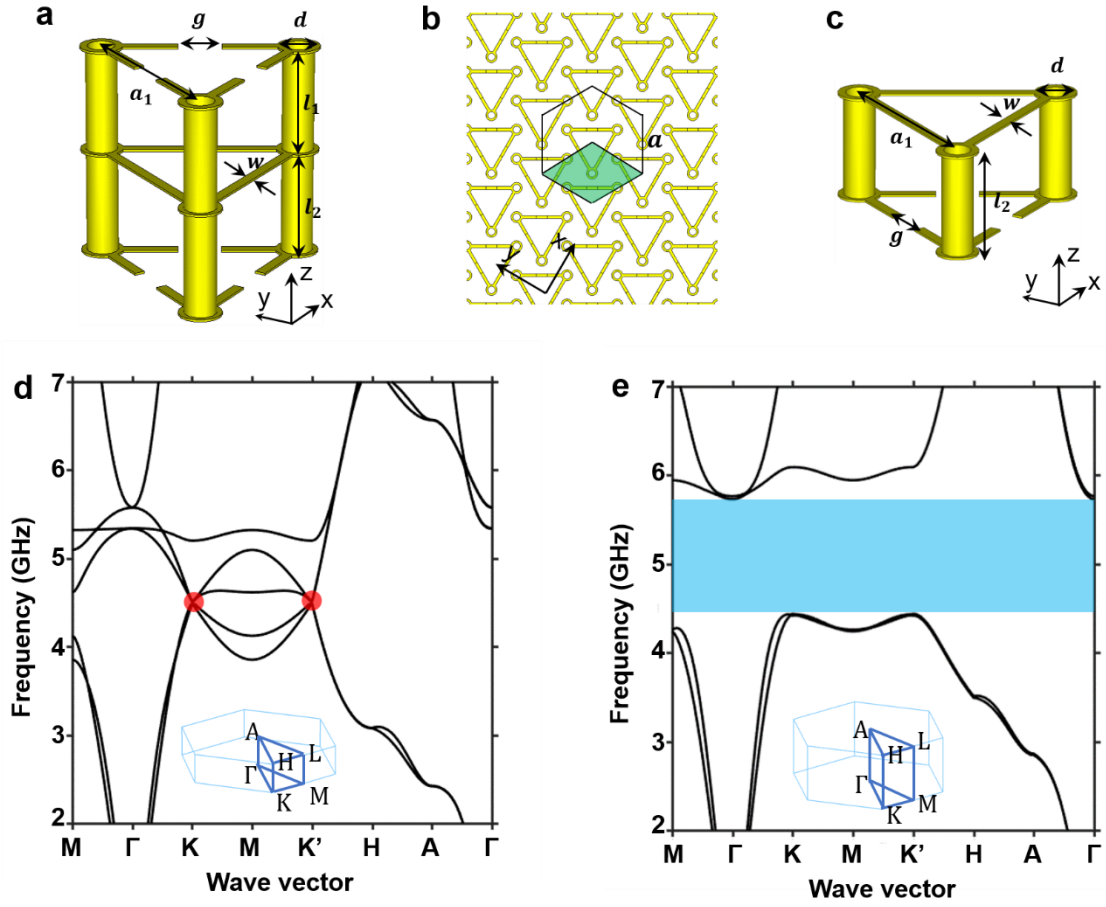


Figure 1. Design of photonic structures with 3D Dirac points and 3D topological bandgap. (a-b) Unit cell and top view of hexagonal lattice with 3D Dirac points. The structure parameters are $l_1 = l_2 = 5$ mm, $g = 2$ mm, $a_1 = 9$ mm, $w = 0.5$ mm, $d = 1.5$ mm, and lattice constant $a = 10.4$ mm. The periodicity in the z direction is 11.3 mm. The background dielectric material has a relative permittivity 2.5. The green rhombus represents a unit cell. (c) Unit cell giving rise to a 3D topological bandgap. The top three SRRs in (a) are removed. The three remaining SRRs have the same geometrical parameters as in (a). The periodicity in the z direction is 5.65 mm. (d-e) Band diagrams of the crystals with unit cells shown in (a) and (c), respectively. Insets show the 3D Brillouin zones for each unit cell. The red dots in (d) are the 3D Dirac points. The blue region in (e) represents the complete topological bandgap.

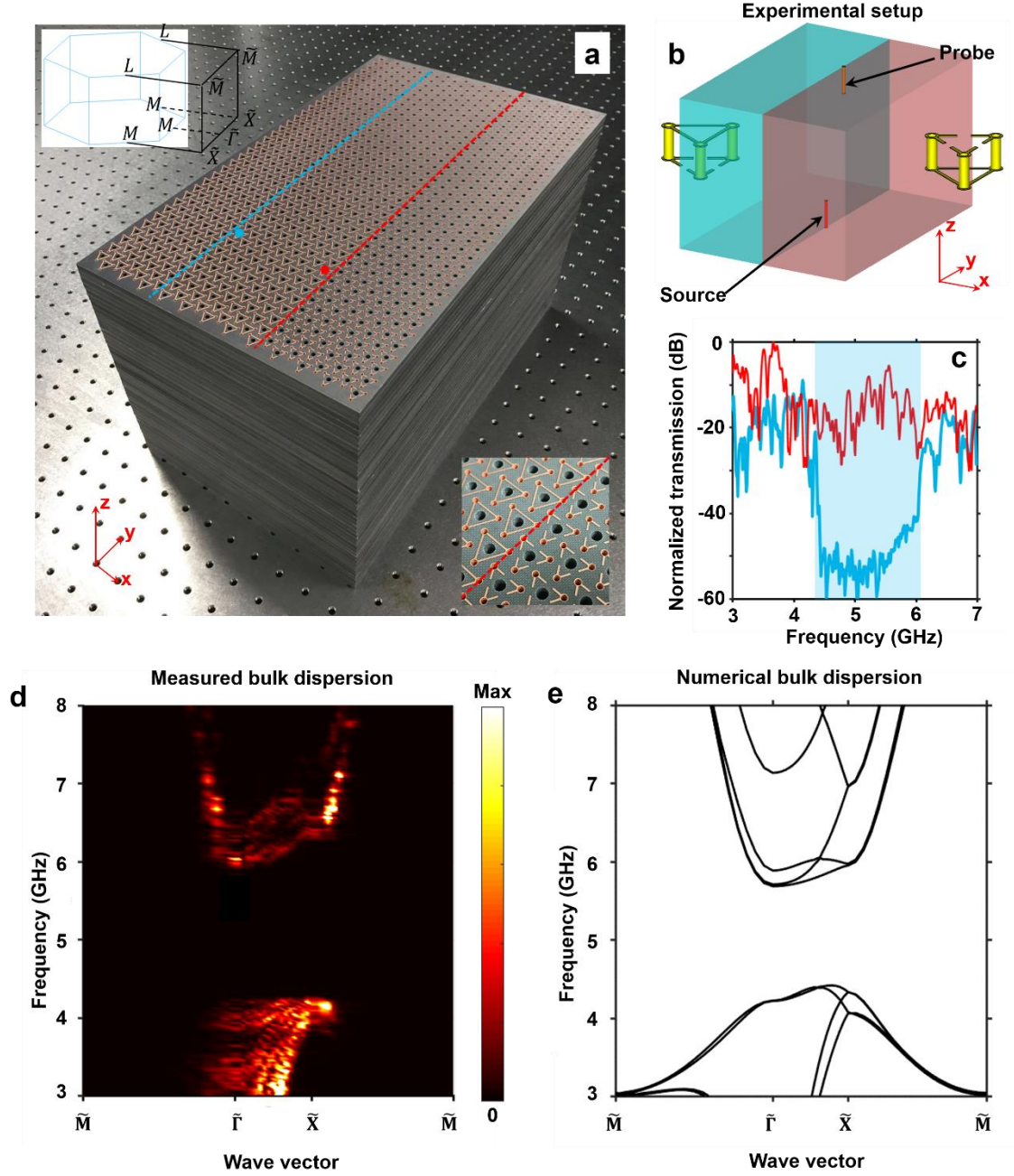


Figure 2. Sample, experimental setup, and measured bulk dispersion of 3D PTI. (a) Photograph of the sample. The blue and red lines indicate the planes used in measuring the bulk and surface states, respectively. Left top inset: projected Brillouin zone for the domain wall. Right bottom inset: photograph of the unit cells near the domain wall. (b) Experimental setup. The source is positioned on the bottom center of the surface, while the probe sweeps the selected plane hole-by-hole. (c) Measured transmissions at the probe point located a depth of 8 unit cells beneath the red (blue) dot. The region highlighted in light blue represents the bulk topological bandgap. (d)-(e) Measured and simulated band diagrams of the 3D PTI, projected on the measurement plane. The color bar in (d) measures the electric energy density.

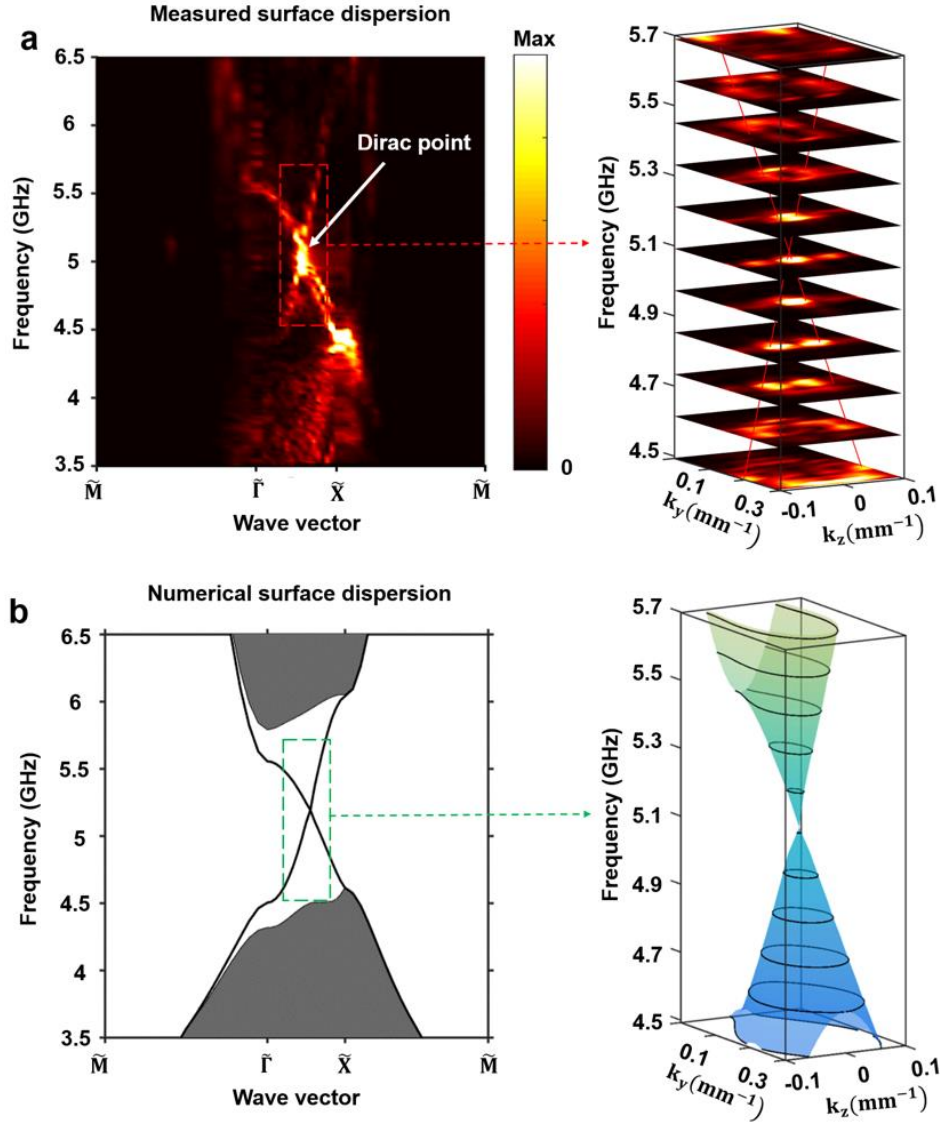


Figure 3. Experimental observation of gapless conical Dirac-like topological surface state of the 3D PTL. (a)-(b) Measured and calculated band diagrams for the topological surface state. Insets: isofrequency contours of the topological surface states at different frequencies. Red lines in (a) are guides to the eye that indicate the shape of the cones that intersect at the Dirac point. Note that there is another Dirac point near the projection of K' , not shown here. The color bar in (a) measures the electric energy density.